Non-strange dibaryons studied in coherent double neutral-meson photoproduction on the deuteron

Takatsugu Ishikawa[1,*], *Hisako* Fujimura[1], *Hiroshi* Fukasawa[1], *Ryo* Hashimoto[1], *Qinghua* He[1], *Yuki* Honda[1], *Takahiro* Iwata[2], *Shun* Kaida[1], *Hiroki* Kanda[3], *Jirohta* Kasagi[1], *Atsushi* Kawano[4], *Shuzo* Kuwasaki[1], *Kazushige* Maeda[3], *Shin'ichi* Masumoto[5], *Manabu* Miyabe[1], *Fusashi* Miyahara[1], *Keiichi* Mochizuki[1], *Norihito* Muramatsu[1], *Akihiko* Nakamura[1], *Ken'ichi* Nawa[1], *Shoei* Ogushi[1], *Yasuyuki* Okada[1], *Ken'yu* Okamura[1], *Yoshihito* Onodera[1], *Kyoichiro* Ozawa[6], *Yasunobu* Sakamoto[4], *Hajime* Shimizu[1], *Hiroyuki* Sugai[1], *Koutaku* Suzuki[1], *Yasuhisa* Tajima[2], *Shin'ichiro* Takahashi[1], *Yusuke* Taniguchi[1], *Yusuke* Tsuchikawa[1], *Hirohito* Yamazaki[1], *Ryuji* Yamazaki[1], and *Hiroshi* Yoshida[2]

[1]Research Center for Electron Photon Science (ELPH), Tohoku University, Sendai 982-0826, Japan
[2]Department of Physics, Yamagata University, Yamagata 990-8560, Japan
[3]Department of Physics, Tohoku University, Sendai 980-8578, Japan
[4]Department of Information Science, Tohoku Gakuin University, Sendai 981-3193, Japan
[5]Department of Physics, University of Tokyo, Tokyo 113-0033, Japan
[6]Institute of Particle and Nuclear Studies, High Energy Accelerator Research Organization (KEK), Tsukuba 305-0801, Japan

Abstract. The $B = 2$ bound/resonance state (dibaryon) is an interesting object, which can be a molecule consisting of two baryons or a spatially compact hexaquark hadron object. The $\gamma d \to \pi^0\pi^0 d$ reaction has been experimentally investigated at incident energies ranging from 0.58 to 1.15 GeV to study non-strange dibaryons. The angular distributions of deuteron emission in the γd center-of-mass energy cannot be reproduced by quasi-free production of two neutral pions followed by deuteron coalescence. Additionally a 2.14-GeV peak is observed in the $\pi^0 d$ invariant mass distribution. These suggest a sequential process such as $\gamma d \to R_{\rm IS} \to \pi^0 R_{\rm IV} \to \pi^0\pi^0 d$ with an isoscalar dibaryon $R_{\rm IS}$ and an isovector dibaryon $R_{\rm IV}$. Since the mass of the observed isoscalar dibaryons are close to the sum of the nucleon (N) and nucleon resonance (N^*) masses, an S-wave NN^* molecule may play a role as a doorway to a dibaryon.

1 Introduction

The structure of hadrons is one of the most important subjects to be studied in the non-perturbative domain of quantum chromodynamics. A $B = 2$ system (dibaryon) is an interesting object to study its basic configuration from a molecule-like state consisting of two baryons such as the deuteron to a spatially-compact hexaquark hadron state. Understanding dibaryons would not only give a clue to the solution of the current problem in hadron physics but also provide an insight into the nuclear equation of state and the interior of a neutron star [1].

The search for dibaryons has a long history [2]. Recent observations of the $d^*(2380)$ dibaryon [3, 4] with $M = 2.37$ GeV, $\Gamma = 0.07$ GeV, and $I(J^\pi) = 0(3^+)$ in the $pn \to \pi^0\pi^0 d$ reaction have opened the door to study non-strange dibaryons. The $d^*(2380)$ may be attributed to a spatially compact hexaquark hadron state and/or an isoscalar $\Delta\Delta$ quasi-bound state $\mathcal{D}_{03}$, which was predicted by Dyson and Xuong [5] as a member of the sextet non-strange dibaryons $\mathcal{D}_{IJ}$ with isospin I and spin J. Many experimental investigations of the sextet members have been made, and candidates for almost all the members are found: the deuteron $\mathcal{D}_{01}$, the $^1S_0$-NN virtual state $\mathcal{D}_{10}$, an isovector ΔN state $\mathcal{D}_{12}$ in the $\pi^+ d \to pp$ reaction [6–9], an isotensor ΔN state $\mathcal{D}_{21}$ in the quasi-free $pp \to \pi^+\pi^- pp$ reaction [10], and an $I = 3$ $\Delta\Delta$ dibaryon $\mathcal{D}_{30}$ in the $pp \to \pi^-\pi^-\pi^+\pi^+ pp$ reaction [11]. However, the dibaryonic interpretations of the experimental data for some members are still questionable.

From now on, we focus on $\mathcal{D}_{12}$ which is a key state of the sextet dibaryons. Experimentally, the evidence for $\mathcal{D}_{12}$ is given as the $^3P_2$ multipole strength at $M = 2.18$ GeV in $\pi^\pm d$ elastic scattering by a partial-wave analysis [7]. The corresponding $^1D_2$-pp amplitude also shows the same structure in the $\pi^+ d \to pp$ reaction [8]. The SAID group provides a pole for $\mathcal{D}_{12}$ [9] from a combined analysis of πd elastic scattering, the $\pi^+ d \to pp$ reaction, and pp elastic scattering. Hoshizaki shows the $\mathcal{D}_{12}$ state is required to explain the pp and πd phase parameters [12], and excludes the interpretation of the state as a cusp or a virtual state [13]. Platonova and Kukulin also claim that conventional meson-exchange models do not explain the $pp \to \pi^+ d$ reaction [14]. Recently, preliminary results for $\mathcal{D}_{12}$ candidates observed in the $\gamma d \to \pi^+\pi^- d$ reaction are reported [15, 16], showing a peak with $M = 2.1$–2.2 GeV and $\Gamma \simeq 0.1$ GeV in both the $\pi^\pm d$ invariant-mass distribu-

*e-mail: ishikawa@lns.tohoku.ac.jp

tions. The peak position is close to the sum of the N and Δ masses, and the width is much narrower than the Δ width. Although these considerations and observations seem to show the existence of $\mathcal{D}_{12}$, a possibility of quasi-free (QF) Δ production cannot be excluded in the interpretation of the experimental data.

There is no doubt that the $\pi^{\pm}d$ system has a resonance-like structure around 2.15 GeV. We study the $\gamma d \to \pi^0\pi^0 d$ reaction, aiming to find and observe $\mathcal{D}_{12}$ in the $\pi^0 d$ subsystem. Possible production mechanisms for the $\gamma d \to \pi^0\pi^0 d$ reaction are classified as follows:

1. dibaryon production: sequential $\pi^0\pi^0$ emission from the deuteron with intermediate isoscalar dibaryon $R_{\rm IS}$ and isovector dibaryon $R_{\rm IV}$ ($\gamma d \to R_{\rm IS} \to \pi^0 R_{\rm IV} \to \pi^0\pi^0 d$).

2. QF-$\pi\pi$ production: $\pi^0\pi^0$ is photoproduced on the QF participant nucleon N_p, followed by coalescence with the spectator nucleon N_s into a deuteron.

3. QF-π production: π^0 is photoproduced on N_p, followed by coalescence with N_s into $R_{\rm IV}$, finally $R_{\rm IV}$ decays into $\pi^0 d$.

4. direct-$\pi\pi$ production: $\pi^0\pi^0$ is directly photoproduced from the deuteron.

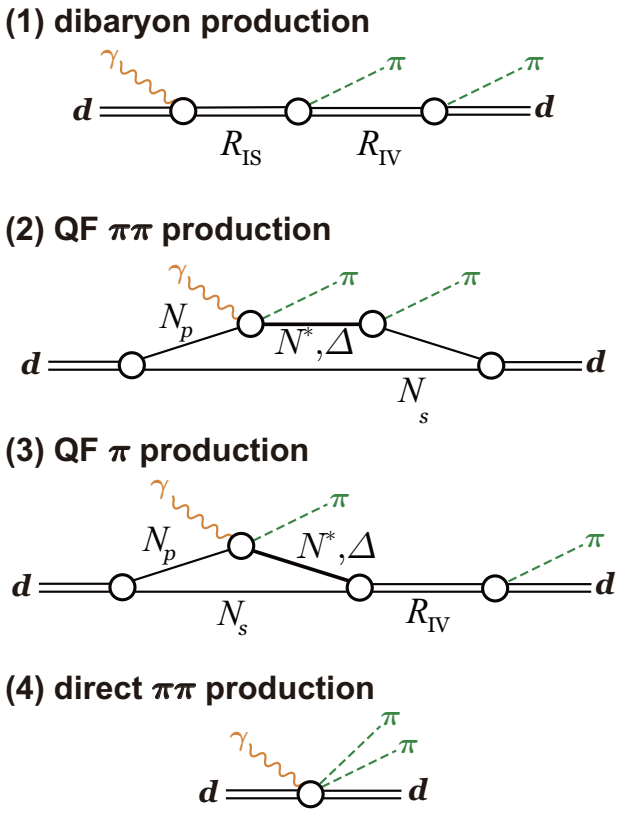

Figure 1. Possible mechanisms for the $\gamma d \to \pi^0\pi^0 d$ reaction. The $R_{\rm IS}$ and $R_{\rm IV}$ denote isoscalar and isovector dibaryons, respectively. The N_p and N_s stand for the participant and spectator nucleons in the quasi-free process, respectively.

In the QF-$\pi\pi$ production mechanism, coalescence into a deuteron requires that the two π^0s should be emitted so as to compensate for the momentum given to N_p. In this case, the angular distribution of deuteron emission in the γd center-of-mass (CM) frame shows strongly backward peaking. As for the QF-π production mechanism, the condition for coalescence into $R_{\rm IV}$ makes the distribution sideway peaking at the incident photon energy around 1 GeV. A completely-different rather-flat distribution is obtained in the dibaryon and direct-$\pi\pi$ production mechanisms. It should be noted that the angular distributions are mainly determined by the deuteron or $R_{\rm IV}$ masses and that the other detailed kinematic conditions do not affect the behaviors of the angular distributions. The most serious background of QF N^* or Δ excitation is kinematically separable from the dibaryon production mechanism.

2 Experiment

A series of meson photoproduction experiments [21] were carried out using the energy-tagged photon beams [22] at the Research Center for Electron Photon Science (ELPH), Tohoku University, Japan. The photon beam was produced by a bremsstrahlung process with a carbon fiber (radiator) with a diameter of 11 μm from the 0.93 and 1.20 GeV circulating electrons in a synchrotron called the STretcher Booster (STB) ring [23]. Each produced photon was energy-tagged by measuring the trajectory of the corresponding post-bremsstrahlung electron with a photon-tagging detector STB-Tagger II in the bending magnet just after the radiator location. The tagging energy of the photon beam ranged from 0.57 to 0.88 and from 0.74 to 1.15 GeV for 0.93- and 1.20-GeV circulating electrons, respectively. The target used in the experiments was liquid deuterium with a thickness of 45.9 mm. The incident photon energies for the two circulating electron energies give γd center of mass energies $W_{\gamma d}$s from 2.38 to 2.61 and from 2.51 to 2.80 GeV. The lowest photon energy for the 0.93-GeV circulating electrons corresponds to the centroid of the $d^*(2380)$ resonance.

All the final-state particles in the $\gamma d \to \pi^0\pi^0 d$ reaction were measured using an electromagnetic calorimeter (EMC) complex, FOREST [24]. FOREST consists of three different EMCs as shown in Fig. 2: the forward EMC consists of 192 pure CsI crystals, the central consists of 252 lead scintillating fiber modules, and the backward consists of 62 lead glass Cherenkov counters, respectively. A plastic scintillator hodoscope (PSH) is placed in front of each calorimeter to identify charged particles. The solid angle of FOREST is approximately 88% in total. The typical photon-tagging rates were 2.8 and 20 MHz, and the photon transmittance ratios (so-called tagging efficiency) were approximately 42% and 53% [22] for the 0.93 and 1.20 circulating electrons, respectively. The trigger condition of the data acquisition (DAQ) was made for detecting more than one final-state particles in coincidence with a photon-tagging signal. The details of the trigger condition are described elsewhere [24]. The average trigger rates were 1.1 and 1.7 kHz, and the average DAQ efficiency

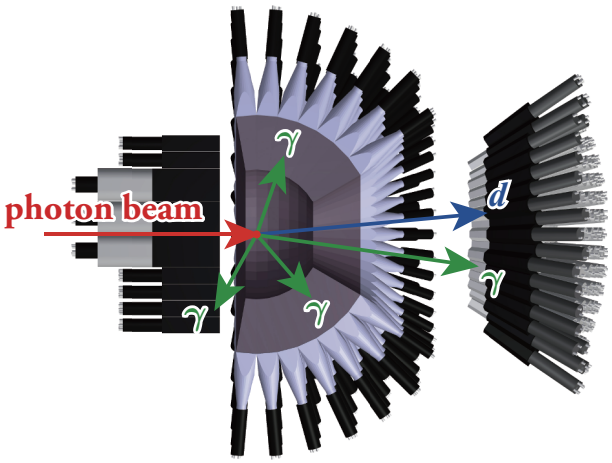

Figure 2. Cross sectional view of FOREST. It consists of three EMCs: the forward (right in the figure), central, and backward (left in the figure) EMCs are comprised of 192 pure CsI crystals, 252 lead scintillating-fiber modules, and 62 lead-glass Cherenkov counters respectively. The energy resolution of each calorimeter is approximately 3% (forward), 7% (central), and 5% (backward) for 1-GeV photons, respectively. A PSH (omitted in the figure) is placed in front of each EMC to identify charged particles.

were 85% and 79% for the 0.93 and 1.20 circulating electrons, respectively.

3 Total cross sections

The analysis of the $\gamma d \to \pi^0\pi^0 d$ reaction was made in the same way as in Refs. [25, 26]. We selected the events containing four neutral particles and a charged particle, and applied a kinematic fit with six constraints: four-momentum conservation, and every $\gamma\gamma$ invariant mass being the π^0 mass. Sideband-background subtraction was performed for accidental-coincidence events detected in STB-Tagger II and FOREST. Events in which the χ^2 probability was higher than 0.4 were selected to reduce those from background processes. The most competitive background process was the QF $\gamma p' \to \pi^0\pi^0 p$ reaction having 100 times higher cross section at maximum [27]. To remove the events from this background process, we made the lower limit of the χ^2 probability relatively higher as 0.4.

The total cross section of the $\gamma d \to \pi^0\pi^0 d$ reaction can be obtained from the equation

$$\sigma = \frac{N_{\pi^0\pi^0 d}}{N'_\gamma N_\tau \eta_{\rm acc} \{{\rm BR}(\pi^0 \to \gamma\gamma)\}^2}, \qquad (1)$$

which uses the number of events for the $\gamma d \to \pi^0\pi^0 d$ reaction $N_{\pi^0\pi^0 d}$, the effective number of incident photons N'_γ, the number of target deuterons per unit area $N_\tau = 0.237$ b^{-1}, the acceptance of the final state $\pi^0\pi^0 d \to \gamma\gamma\gamma\gamma d$ detection $\eta_{\rm acc}$, and the branching ratio of the neutral pion to the two-photon decay BR($\pi^0 \to \gamma\gamma$). The number of incident photons N_γ is determined by multiplying the number of photon-tagging signals after the counting-loss correction by the corresponding photon transmittance. The N'_γ is a product of multiplying N_γ and the DAQ efficiency. The acceptance of $\gamma\gamma\gamma\gamma d$ detection is estimated by a Monte-Carlo simulation based on Geant4 [28]. Here, the event generation is modified from pure phase-space generation to reproduce the following three measured distributions: the $\pi\pi$ invariant mass $M_{\pi\pi}$, the πd invariant mass $M_{\pi d}$, and the deuteron emission angle $\cos\theta_d$ in the γd-CM frame. Fig. 3 shows the total cross section σ as a function of the γd CM energy $W_{\gamma d}$. The systematic uncertainty of σ includes the uncertainty of event selection in the kinematic fit, that of acceptance owing to the uncertainties of the $M_{\pi\pi}$, $M_{\pi d}$, and $\cos\theta_d$ distributions in event generation of the simulation, that of detection efficiency of deuterons, and that of normalization resulting from the numbers of target deuterons and incident photons.

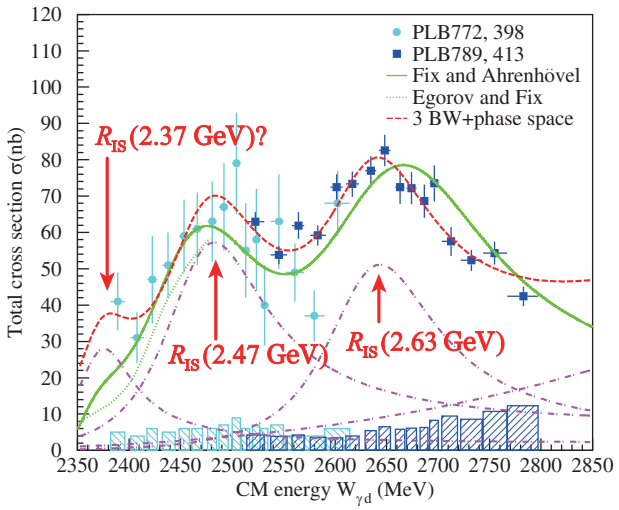

Figure 3. Total cross section σ as a function of $W_{\gamma d}$. The circles (cyan) and squares (blue) show σs obtained in Ref. [25] and in Ref. [26], respectively. The horizontal error of each data point corresponds to the coverage of the incident photon energy, and the vertical error shows the statistical error of σ. The solid and dotted curves (green) show theoretical calculations given in Ref. [19] and in Ref. [20] based on the QF-$\pi\pi$ production mechanism, respectively. The dashed curve (red) shows the fitted function (5) expressed by a sum of three Breit-Wigner peaks and phase-space contributions. Each contribution is shown in a dashed dotted curve (red). The lower hatched histograms show the systematic errors of σ.

The excitation function is not monotonically increasing but shows resonance-like behavior peaked at around 2.47 and 2.63 GeV. The two-peak structure is similar to the excitation function of the $\gamma N \to \pi^0\pi^0 N$ reaction with two peaks at the γN-CM energy $W_{\gamma N}$ of ~1.5 and ~1.7 GeV [17, 18], corresponding to the second- and third-resonance regions of the nucleon. A naive interpretation of this behavior may be a QF excitation of the nucleon in the deuteron, followed by coalescence into the deuteron. The solid curve in Fig. 3 shows a calculation performed by Fix and Ahrenhövel (FA) based on the QF-$\pi\pi$ produc-

tion mechanism [19]. The calculation reproduces the data surprisingly well. A calculation performed by Egorov and Fix based [20] on the QF-$\pi\pi$ mechanism also gives a similar excitation function as shown in Fig. 3 (dotted curve). However, as discussed later in section 4.2, the kinematic condition for the obtained data completely differs from the QF-$\pi\pi$ and QF-π production mechanisms.

Although the measured cross sections are well-reproduced in the FA calculation, the discrepancy seems observed in the lowest incident photon energy region (~0.57 GeV). This discrepancy may be explained by excitation of the $d^*(2380)$ dibaryon resonance. The $d^*(2380)$ contribution is estimated by fitting the function

$$\sigma(W_{\gamma d}) = \sigma_{d^*}\mathrm{BW}(W_{\gamma d}) + \sigma_{\mathrm{FA}}(W_{\gamma d}) \quad (2)$$

to the data obtained for the 0.92 GeV circulating electrons, where $\mathrm{BW}(W_{\gamma d})$ denotes the relativistic Breit-Wigner function [29] corresponding to the expected $d^*(2380)$ contribution with a centroid of $M = 2.37$ GeV and a width of $\Gamma = 68$ MeV. The σ_{FA} stands for the total cross section in the FA calculation. The χ^2/dof of the fit is 10.1/15, and the obtained parameter is

$$\sigma_{d^*} = 18.4 \pm 9.2 \text{ nb}. \quad (3)$$

The $d^*(2380)$ contribution is not statistically significant, and the upper limit of the total cross section is found to be 34 nb at $W_{\gamma d} = 2.37$ GeV (90% confidence level).

4 Differential cross sections

The differential cross sections, $d\sigma/dM_{\pi\pi}$, $d\sigma/dM_{\pi d}$, and $d\sigma/d\Omega_d$, are obtained for each group of photon-tagging channels divided into four groups. All the differential cross sections obtained are plotted in Fig. 2 in Ref. [26]. Here, we focus on the $M_{\pi d}$ and $d\sigma/d\Omega_d$ distributions for the highest photon-tagging group. The $M_{\pi d}$ distribution is investigated to determine the mass and width of a peak near 2.15 GeV. The differential cross section as a function of the deuteron emission angle $d\sigma/d\Omega_d$ is shown to study the reaction mechanism for the $\gamma d \to \pi^0\pi^0 d$ reaction.

4.1 $M_{\pi d}$ distribution

The $M_{\pi d}$ distribution shows two peaks for the higher incident photon energies. The centroid of the low-mass peak is ~ 2.15 GeV independently of the incident energy. However, that of the high-mass peak decreases with a decrease in the incident energy, and finally the two peaks are merged into a bump. The high-mass peak reflects the appearance of the 2.15-GeV peak in the $M_{\pi d}$ distribution between the other pion and deuteron (reflection). This interpretation becomes obvious by looking at the correlation between the two $M_{\pi d}$s (see Fig. 3(b) in Ref. [26]). The $M_{\pi d}$ distribution of the FA calculation shown in Fig. 4 (dotted) also shows a similar distribution having two peaks, which are caused by QF $\pi^0\Delta$ production.

We have analyzed the $M_{\pi d}$ distribution in detail. We consider the sequential (dibaryon and QF-π production mechanisms) and non-sequential (QF-$\pi\pi$ and direct-$\pi\pi$ production meachisms) processes of two-π^0 emission. Here, the contribution from the latter process is assumed to be proportional to the phase space. The mass and width are determined by fitting a function, expressed as a sum of a Breit-Wigner (BW) peak, its reflection, and phase-space contributions, to the $M_{\pi d}$ data. The function is given by convolution of a Gaussian with an experimental mass resolution of $\sigma_M = 0.011$ GeV, and

$$N(m_1) = \int_{m_2} \left(\alpha \left| A^L_{M,\Gamma}(m_1) + A^L_{M,\Gamma}(m_2) \right|^2 + C \right) \times V_{\mathrm{PS}}(m_1, m_2)\, dm_2, \quad (4)$$

where $V_{\mathrm{PS}}(m_1, m_2)$ expresses the phase-space contribution, $A^L_{M,\Gamma}(m) = \left(m^2 - M^2 + iM\Gamma\right)^{-1}$ represents the BW amplitude with mass M and width Γ. The acceptance is taken into account depending on $M_{\pi\pi}$, $M_{\pi d}$, and $\cos\theta_d$ to estimate $V_{\mathrm{PS}}(m_1, m_2)$. The parameters obtained are $M = 2.14 \pm 0.01$ GeV and $\Gamma = 0.09 \pm 0.01$ GeV. The mass is slightly lower than the sum of the N and Δ masses (~ 2.17 GeV), and the width is narrower than that of Δ (~ 0.12 GeV) [30]. It should be noted that the FA calculation does not reproduce the $M_{\pi d}$ distribution, either. The centroid of the second peak is higher at higher incident energy.

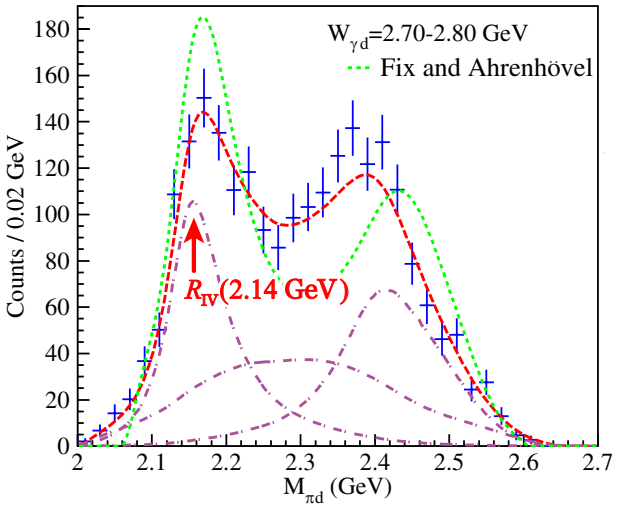

Figure 4. Typical πd invariant mass $M_{\pi d}$ distribution. The dashed curves (red) show the fitted functions, expressed as a sum of a Breit-Wigner (BW) peak, its reflection, and phase-space contributions, to the data. Contributions of a BW peak and its reflection are summed up at an amplitude level. Each contribution is plotted in a dashed dotted curve (magenta). The dotted curve (green) correspond to the FA calculations with arbitrary normalization.

4.2 Angular distribution of deuteron emission

A great difference between the FA calculation based on the QF-$\pi\pi$ mechanism and the experimental data appears in the angular distribution of deuteron emission $d\sigma/d\Omega_d$ in Fig. 5. The experimentally obtained $d\sigma/d\Omega_d$ shows

a gradually-increasing behavior with decrease of $\cos\theta_d$. While the FA calculation based on the QF-$\pi\pi$ production mechanism provides a strongly backward-peaking behavior. The QF-π production mechanism, giving a sideway peak in $d\sigma/d\Omega_d$ at high incident energies in Fig. 5 (dotted curve in magenta), is also rejected. A sideway peak corresponding to the QF-π production mechanism is not observed in the experimental distribution. Since neither backward nor sideway peaks are not observed in the $d\sigma/d\Omega_d$ distribution, the sequential and non-sequential processes in section 4 one-to-one correspond to the dibaryon and direct-$\pi\pi$ production mechanisms, respectively.

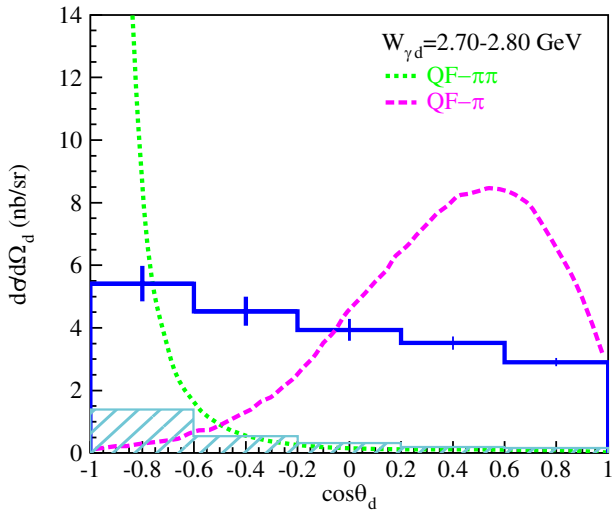

Figure 5. Typical differential cross section $d\sigma/d\Omega_d$. The dotted (green) and dashed (magenta) curves show $d\sigma/d\Omega_d$ as a function of $\cos\theta_d$ for the QF-$\pi\pi$ and QF-π mechanisms, respectively, where their yields are normalized so that the total cross section should be the same. The lower hatched histogram shows the systematic errors of $d\sigma/d\Omega_d$.

We conclude that the peak at 2.14 GeV in the $M_{\pi d}$ spectrum is attributed to a dibaryon state, which can be generated in neither the QF-$\pi\pi$ production mechanism nor the QF-π production mechanism. This conclusion gives the dominant sequential process $\gamma d \to R_{\rm IS} \to \pi^0 R_{\rm IV} \to \pi^0\pi^0 d$, and motivates the following interpretation for the resonance-like structure in Fig. 3: a dibaryon state can be formed from a deuteron and a photon; the generated state may be a loosely-coupled molecular state; it plays a role as a doorway to a more complicated dibaryon state. Of particular importance is the fact that there is no spectator nucleon in the observed reaction. We fit a function expressed by a sum of three BW peaks and phase-space contributions to the data. The function is given by

$$\sigma(W_{\gamma d}) = \sigma_{\rm PS}(W_{\gamma d})\left\{1 + \sum_{i=0}^{2} \alpha_i L_{M_i,\Gamma_i}(W_{\gamma d})\right\}, \quad (5)$$

where $\sigma_{\rm PS}(W_{\gamma d})$ denotes σ for the phase-space contribution, $L_{M,\Gamma}(W_{\gamma d})$ represents a BW function with the centroid of M and width of Γ. Here, three BW peaks are summed up at a cross section level. The M_0 = 2.37 GeV and Γ_0 = 0.07 GeV are fixed to the values for $d^*(2380)$ [4], and the absolute values for $\sigma_{\rm PS}(W_{\gamma d})$ are determined to fit the phase-space component in each $M_{\pi d}$ spectrum (see Fig. 4). The fitted function and each contribution to it are also plotted in Fig. 3 (dashed-and-dotted curve in magenta). The obtained parameters for the two peaks are (M_1, Γ_1) = (2.47, 0.12) GeV and (M_2, Γ_2) = (2.63, 0.13) GeV. Isoscalar dibaryons appear not only at 2.37 GeV but also at 2.47 and 2.63 GeV. It should be noted that each observed peak may be comprised of several overlapping resonances and that the WASA-at-COSY data covering masses up to 2.56 GeV do not show any signature of the 2.47-GeV dibaryon.

5 Spin-parity

Information on the spin-parity of the dibaryon states has been deduced from angular distributions of π^0s obtained for the events from $M_{\pi d}$ = 2.05–2.25 GeV in Fig. 4. We define π_1 and π_2 as follows: π_2 is one of the two pions giving $2.05 \le M_{\pi d} < 2.25$ GeV, and π_1 is the other pion. Here, we assume π_1 is emitted first in the dominant dibaryon production mechanism, leaving the $\pi_2 d$ system with $2.05 \le M_{\pi d} < 2.25$ GeV, and π_2 is emitted subsequently. We combine the data of the two highest-energy groups, which covers $W_{\gamma d}$ from 2.66 to 2.80 GeV, to analyze angular distributions. Thus, we expect the reaction sequence $\gamma d \to R_{\rm IS}(2.63\ {\rm GeV}) \to \pi_1 R_{\rm IV}(2.14\ {\rm GeV}) \to \pi_1\pi_2 d$ together with the direct $\pi_1\pi_2$ production mechanism. Fig. 6(a) shows the deduced π_1 angular distribution after the acceptance correction is applied in the γd-CM frame with the z axis taken along the incident photon direction. The experimental distribution is well-reproduced by a sum of two terms, constant and proportional to $\cos\theta$. This $\cos\theta$ dependence can be understood as a result of interference between π_1-emission amplitudes with different parities. The π_2 angular distribution in the rest frame of the $\pi_2 d$ system (π_1-π_2 angular correlation) after the acceptance correction is applied is shown in Fig. 6(b), where the z axis is defined to be opposite to the direction of π_1 emission. Unlike Fig. 6(a), the distribution shows almost 90° symmetry. This implies that the 2.14-GeV resonance is made of a single J^π state or mixed states with the same parity (no interference between different parities). The FA calculation (provided in the same kinematic condition) completely fails to reproduce both the angular distributions, due to the difference in the underlying reaction mechanism as discussed previously (QF-$\pi\pi$ production mechanism adopted in the FA calculation is not observed in the experiment). A sharp peak at 0° in Fig. 6(a) is the reflection of the backward peak in $d\sigma/d\Omega_d$. In Fig. 6(b), the distribution takes an upward-convex shape being opposite to the experiment.

We calculate the π_1 and π_2 angular distributions for the reaction sequence $\gamma d \to R_1 \to \pi_1 R_2 \to \pi_1\pi_2 d$ using the density matrix (statistical tensor) formalism [31], where spins of R_1 and R_2 are denoted by J_1 and J_2, respectively. The formalism incorporates the exchange symmetry between π_1 and π_2. A possible contribution from

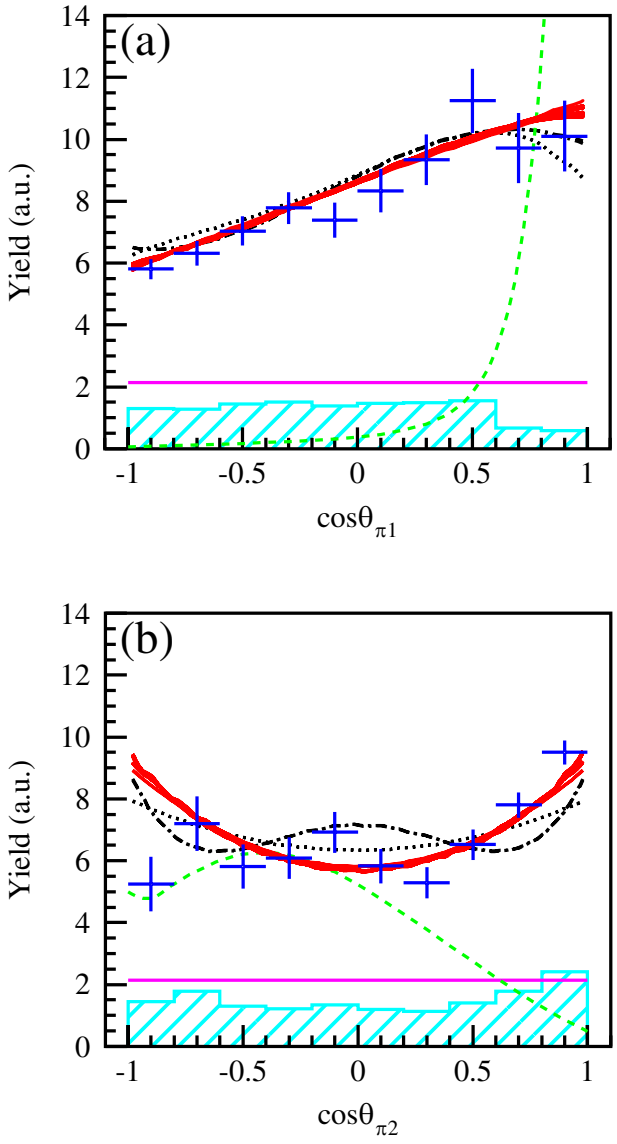

Figure 6. Acceptance-corrected angular distributions for π_1 in the γd-CM frame (z axis: the photon beam direction) (a), and for π_2 in the $\pi_2 d$ rest frame (z axis: the opposite direction to π_1) (b). Events with $M_{\pi_2 d}$ = 2.05–2.25 GeV and $W_{\gamma d}$ = 2.66–2.80 GeV are selected. The lower hatched histograms (cyan) show the corresponding systematic errors. The dashed curves (green) show the corresponding distributions in the FA calculations. The angular distributions are plotted with a shaded band (red) for $J^\pi_2 = 1^+$, 2^+, and 3^-, and with dotted and dash-dotted curves (black) for $J^\pi_2 = 1^-$ and 2^-, respectively. The solid horizontal lines (magenta) show the phase-space contributions.

non-sequential direct $\pi^0\pi^0$ production mechanism is assumed to be proportional to the phase-space contribution, of which the fraction is determined from the $M_{\pi d}$ spectrum in Fig. 4 for each photon-tagging group. Since the π_2 angular distribution is almost symmetric with respect to $\cos\theta_{\pi_2} = 0$, the interference effect may be small. Thus, the contributions from the sequential dibaryon production and non-sequential direct $\pi^0\pi^0$ production mechanisms are summed up incoherently. A set of the amplitudes of sequential processes $A_{\Lambda\Lambda}$ is determined for all the $\Lambda = (L_0, J_1, L_1, J_2, L_2)$ combinations to reproduce the measured π_1 and π_2 angular distributions simultaneously (20 data points), where L_0, L_1, and $L_2 \leq 2$ denote angular momenta carried by the incident photon, π_1 emission, and π_2 emission, respectively. An amplitude for a mixed state is given by $A_{\Lambda\Lambda'} = (A_{\Lambda\Lambda} A_{\Lambda'\Lambda'})^{1/2}$. The S-wave NN^* molecular states are assumed to play a role as a doorway to R_1 since all the observed isoscalar dibaryons are close to the sum of NN^* masses as discussed in section 6. Here, the considered N^*s are $D_{15}(1675)$, $F_{15}(1680)$, and $P_{13}(1720)$, which give dominant contributions in the $\gamma N \to \pi^0\pi^0 N$ reaction in the relevant energy region [18]. Hence, J^π_1s under consideration are 1^+, $2^\pm$, and $3^\pm$. Additionally, R_2 is assumed to be a single resonance, namely $J_2 = J'_2$ and $L_2 = L'_2$.

In Fig. 6, also shown are the angular distributions calculated for $J^\pi_2 = 1^\pm$, $2^\pm$, and 3^+. The $J^\pi_2 = 0^\pm$ assignments are already excluded because of an isotropic distribution for π_2 emission. The assignments of $J^\pi_2 = 1^+$, 2^+, and 3^- show almost the same quality to reproduce the angular distributions ($29 < \chi^2 < 32$). We reject the $J^\pi_2 = 1^-$ and 2^- assignments, giving worse distributions ($\chi^2 = 47$ and 55), respectively, with a confidence level of higher than 99.7% (3σ), and leave the possibility of $J^\pi_2 = 1^+$, 2^+ and 3^-. Regarding J^π_1, major components are 1^+ (~70%) and 2^- (~20%) for the case of $J^\pi_2 = 1^+$ and 2^+, while they are distributed widely to $J^\pi_1 = 1^+$, $2^\pm$, and 3^+ for $J^\pi_2 = 3^-$. The $J^\pi_2 = 2^+$ assignment not only coincides with the energy dependence of the $^3P_2$-πd amplitude, but also supports the existence of the predicted $\mathcal{D}_{12}$ state at 2.14 GeV. The $J^\pi_2 = 3^-$ assignment is consistent with the energy dependence of the $^3D_3$-πd amplitude (about a half strength of $^3P_2$). There is no experimental sign for a 1^+ state, although two isovector 0^- and 2^- states at 2.2 GeV have been reported recently [32]. Most probably, $R_{\rm IS}(2.63$ GeV) is a mixing state between $J^\pi_1 = 1^+$ (~70%) and 2^- (~20%), and $J^\pi_2 = 2^+$ for $R_{\rm IV}(2.14$ GeV).

6 Discussion

A rather-flat angular distribution of deuteron emission completely differs from the QF-$\pi\pi$ and QF-π production mechanisms. In addition, the $M_{\pi d}$ distributions shows a peak at 2.14 GeV. The present work suggests a sequential process $\gamma d \to R_{\rm IS} \to \pi^0 R_{\rm IV} \to \pi^0\pi^0 d$ is dominant with two 2.47- and 2.63-GeV $R_{\rm IS}$ and a 2.14-GeV $R_{\rm IV}$. Fig. 7 shows the deuteron hadronic excited spectrum. The three $R_{\rm IS}$s are photo-excited from the deuteron with masses of 2.37, 2.47, and 2.63 GeV. The spin-parity of $R_{\rm IS}(2.37$ GeV) is 3^+, and that of $R_{\rm IS}(2.63$ GeV) is found to be most probably a mixing of 1^+ and 2^-. The $R_{\rm IS}(2.63$ GeV) decays into $R_{\rm IV}(2.14$ GeV) by emitting π^0 with angular momenta of 0 and 1, and the $R_{\rm IV}(2.14$ GeV) decays into the deuteron by emitting π^0 with an angular momentum of 1.

The sum of the nucleon N and $N(1440)P_{11}$ nucleon resonance masses (the $NN(1440)P_{11}$ mass) is very close to the $R_{\rm IS}(2.37$ GeV) mass. The masses of $NN(1535)S_{11}$ and $NN(1520)D_{13}$ masses are close to the

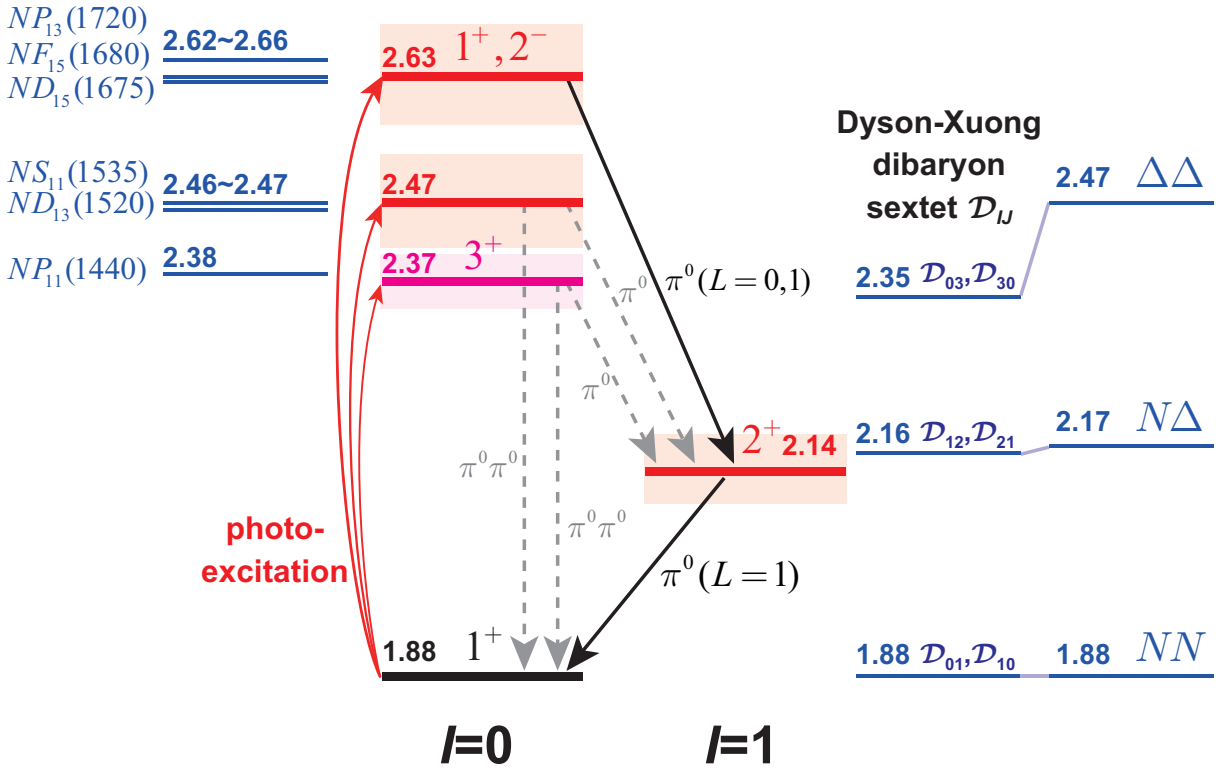

Figure 7. Deuteron hadronic excitation spectrum. The three R_{IS}s are photo-excited from the deuteron with masses of 2.37, 2.47, and 2.63 GeV. The spin-parity of R_{IS}(2.37 GeV) is 3^+, and that of R_{IS}(2.63 GeV) is found to be a mixing of 1^+ and 2^-. The R_{IS}(2.63 GeV) decays into R_{IV}(2.14 GeV) by emitting π^0 with angular momenta of 0 and 1, and the R_{IV}(2.14 GeV) decays into the deuteron by emitting π^0 with an angular momentum of 1. The left-side levels show the sum of the nucleon and nucleon resonance masses, and the right-side levels show the masses of the dibaryon sextet member predicted by Dyson and Xuong [5], and the sum of the two baryon masses.

R_{IS}(2.47 GeV) mass. The $NN(1675)D_{15}$, $NN(1680)F_{15}$, and $NN(1720)P_{13}$ masses are close to the R_{IS}(2.63 GeV) mass. Thus, we consider the possibility that the S-wave NN^* molecular states may play a role as a doorway to the three R_{IS} states.

The R_{IS}(2.37 GeV), or $d^*(2380)$, has been considered as a mixing state between a spatially compact hexaquark hadron state and an isoscalar $\Delta\Delta$ quasi-bound state. The R_{IV} would be also attributed to be the $N\Delta$ quasi-bound state since its mass is lower than the $N\Delta$ mass, and its width is narrower than that of Δ. The dibaryon sextet picture predicted by Dyson and Xuong [5] is now established owing to strong evidence for the existence of the 2.14-GeV isovector dibaryon in the $\pi^0 d$ channel. Additionally, our work shows evidence of the 2.47 and 2.63-GeV isoscalar dibaryons in the $\pi^0\pi^0 d$ channel. These findings would give a base to explore dibaryon states lying at higher masses.

To study dibaryon states, it is advantageous to find two neutral mesons and the deuteron in the final state. The $\gamma d \to \pi^0\eta d$ reaction also satisfy this condition. The angular distribution of deuteron emission in this reaction also shows rather flat, suggesting dibaryon production mechanism seems dominant. Since the available phase space is very limited in this reaction at incident energies below 1.2 GeV, it is difficult to determine the mass, width, and spin-parity of the intermediate dibaryon states using the current data. The maximum energy for circulating electrons in the synchrotron at ELPH has increased after the 2011 earthquake, allowing us to study the $\gamma d \to \pi^0\eta d$ reaction in more detail.

7 Summary

The total and differential cross sections have been measured for the $\gamma d \to \pi^0\pi^0 d$ reaction at E_γ = 0.75–1.15 GeV. The measured angular distribution of deuteron emission is rather flat, suggesting that a sequential process $\gamma d \to R_{IS} \to \pi^0 R_{IV} \to \pi^0\pi^0 d$ is dominant. The total cross section σ as a function of $W_{\gamma d}$ shows isoscalar dibaryons R_{IS} with masses of 2.47 and 2.63 GeV. The σ for R_{IS} with a mass of 2.37 GeV corresponding to the $d^*(2380)$ dibaryon observed by the WAST-at-COSY collaboration is found to be 18.4 ± 9.2 nb at the central mass. The $\pi^0 d$ invariant-mass distributions show an isovector dibaryon R_{IV} with a mass of 2.14 GeV. Most probably, R_{IS}(2.63 GeV) is interpreted as a mixing state between $J^\pi_1 = 1^+$ (~70%) and 2^- (~20%), and $J^\pi_2 = 2^+$ for R_{IV}(2.14 GeV). The details of the analysis and discussion can be found elsewhere [26].

Acknowledgments

The authors express their gratitude to the ELPH accelerator staff for stable operation of the accelerators in the FOREST experiments. They acknowledge Mr. Kazue Matsuda, Mr. Ken'ichi Nanbu, and Mr. Ikuro Nagasawa for their technical assistance in the FOREST experiments. They also thank Prof. Alexander I. Fix for the theoretical calculations of the cross sections and fruitful discussion. This work was supported in part by JSPS KAKENHI Grants Nos. 17340063, 19002003, 24244022, 26400287, 16H02188, 19H01902, and 19H05141.

References

[1] A. Akmal, V.R. Pandharipande, D.G. Ravenhall, Phys. Rev. C **58**, 1804 (1998).
[2] H. Clement, Prog. Part. Nucl. Phys. **93**, 195 (2017).
[3] M. Bashkanov *et al.* (CELSIUS/WASA collaboration), Phys. Rev. Lett. **102**, 052301 (2009).
[4] P. Adlarson *et al.* (WASA-at-COSY collaboration), Phys. Rev. Lett. **106**, 242302 (2011).
[5] F.J. Dyson, N.-H. Xuong, Phys. Rev. Lett. **13**, 815 (1964).
[6] B.S. Neganov, L.B. Parfenov, J. Exp. Theor. Phys. **7**, 528 (1958).
[7] R.A. Arndt, I.I. Strakovsky, R.L. Workman, Phys. Rev C. **50**, 1796 (1994).
[8] R.A. Arndt, I.I. Strakovsky, R.L. Workman, D.V. Bugg, Phys. Rev C. **48**, 1926 (1993).
[9] C.H. Oh, R.A. Arndt, I.I. Strakovsky, R.L. Workman, Phys. Rev C. **56**, 635 (1997).
[10] P. Adlarson *et al.* (WASA-at-COSY collaboration), Phys. Rev. Lett. **121**, 052001 (2018),
[11] P. Adlarson *et al.* (WASA-at-COSY collaboration), Phys. Lett. B **762**, 455 (2016).
[12] N. Hoshizaki, Phys. Rev C. **45**, R1424 (1992); Prog. Theor. Phys. **89**, 251 (1992); Prog. Theor. Phys. **89**, 563 (1992).
[13] N. Hoshizaki, Prog. Theor. Phys. **89**, 569 (1992).
[14] M.N. Platonova, V.I. Kukulin, Phys. Rev. C **94**, 054039 (2016).
[15] R.A. Schumacher, talk at YITP workshop "Meson in Nucleus 2016" (MIN16) (2016); MIN16 website: ⟨http://www2.yukawa.kyoto-u.ac.jp/~min2016/⟩.
[16] H. Kanda, talk at ELPH workshop "Meson Production and Meson-Baryon Interaction" (MPMBI) (2015); MPMBI website: ⟨http://www.lns.tohoku.ac.jp/workshop/c013/⟩.
[17] Y. Assafiri, et al. (GRAAL collaboration), Phys. Rev. Lett. **90**, 222001 (2003); J. Ajaka, et al. (GRAAL collaboration), Phys. Lett. B **651**, 108 (2007).
[18] M. Dieterle, et al. (A2 collaboration), Eur. Phys. J. A **51**, 142 (2015).
[19] A. Fix, H. Arenhövel, Euro. Phys. J. A **25**, 115 (2005).
[20] M. Egorov, A. Fix, Nucl. Phys. A 933 (2015) 104.
[21] T. Ishikawa *et al.*, JPS Conf. Proc. **10**, 031001 (2016); PoS (Hadron 2013) **095** (2013); Few Body Sys. **54**, 1047 (2013).
[22] T. Ishikawa *et al.*, Nucl. Instrum. Meth. A **622**, 1 (2010); **811**, 124 (2016); Y. Matsumura *et al.*, Nucl. Instrum. Meth. A **902**, 103 (2018); Y. Obara *et al.*, Nucl. Instrum. Meth. A **922**, 108 (2019).
[23] F. Hinode, et al., in: Proceedings of 2005 Particle Accelerator Conference (2005) 2458.
[24] T. Ishikawa, et al., Nucl. Instrum. Meth. A **832**, 108 (2016).
[25] T. Ishikawa, et al., Phys. Lett. B **772**, 398 (2017).
[26] T. Ishikawa, et al., Phys. Lett. B **789**, 413 (2019).
[27] B. Krusche *et al.*, Eur. Phys. J. A **324**, 309 (1999).
[28] S. Agostinelli *et al.*, Nucl. Instrum. Meth. A **506**, 250 (2003); J. Allison *et al.*, IEEE Trans. on Nucl. Sci. **53**, 270 (2006); Geant4 website ⟨http://geant4.cern.ch/⟩.
[29] A.R. Bohm, Y. Sato, Physical Review D 71 (2005) 085018.
[30] C. Patrignani *et al.* (Particle Data Group), Chin. Phys. C **40**, 100001 (2016).
[31] L.C. Biedenharn, M.E. Rose, Rev. Mod. Phys. **25**, 729 (1953).
[32] V. Komarov, D. Tsirkov, et al., Phys. Rev. C **93**, 065206 (2016).